# Cs2AgBiBr6 as a mixed anion perovskites for photovoltaic applications: A first-principle study

**Article** *in* Materials Today: Proceedings · July 2022

DOI: 10.1016/j.matpr.2022.06.063



**6 authors**, including:

Håkon Eidsvåg
Høgskulen på Vestlandet
**6** PUBLICATIONS **93** CITATIONS
SEE PROFILE

Arunasalam Thevakaran
University of Jaffna
**9** PUBLICATIONS **26** CITATIONS
SEE PROFILE

Punniamoorthy Ravirajan
University of Jaffna
**107** PUBLICATIONS **2,433** CITATIONS
SEE PROFILE

Materials Today: Proceedings 64 (2022) 1783–1788

Contents lists available at ScienceDirect

Materials Today: Proceedings

journal homepage: www.elsevier.com/locate/matpr

# $Cs_2AgBiBr_6$ as a mixed anion perovskites for photovoltaic applications: A first-principle study

W.A. Chapa Pamodani Wanniarachchi [a,b], Håkon Eidsvåg [b], Thevakaran Arunasalam [a], Punniamoorthy Ravirajan [a], Dhayalan Velauthapillai [b], Ponniah Vajeeston [c,*]

[a] Clean Energy Research Laboratory (CERL), Department of Physics, University of Jaffna, Jaffna 40000, Sri Lanka
[b] Faculty of Engineering, Western Norway University of Applied Sciences, 5020 Bergen, Norway
[c] Department of Chemistry, Center for Materials Science and Nanotechnology, University of Oslo Box 1033, Blindern, N-0315 Oslo, Norway

ARTICLE INFO

*Article history:*
Available online 8 July 2022

*Keywords:*
$Cs_2AgBiBr_6$
Optoelectronic properties
Bandgap
Cubic
Tetragonal

ABSTRACT

*Ab initio* calculations were performed for cubic Fm-3 m (225) and tetragonal (I4/m) phases for $Cs_2AgBiBr_6$(CaB2). We used the Vienna Ab Initio Simulation Package (VASP) to calculate the ground state properties using two different exchange-correlation functionals, namely the Generalized gradient approximation method (GGA) and the screened hybrid functional as proposed by Heyd, Scuseria, and Ernzerhof (HSE06) method. Tetragonal $Cs_2AgBiBr_6$ phase was stabilized in the tetragonal phase. The bandgap ($E_g$) was calculated using HSE06 for the polymorphs optimized at the PBE level and it is found that they belong to the indirect bandgap. The calculated bandgap for cubic and tetragonal phases in HSE06 for $Cs_2AgBiBr_6$ were 1.97 eV, and 2.4 eV, respectively. The character of chemical bonding in $CaB_2$ is discussed based on electronic structures, charge density, charge transfer, and bond overlap population analyses.

Selection and peer-review under responsibility of the scientific committee of the Functional Materials for Energy, Environment and Biomedical Applications.

## 1. Introduction

Crystalline silicon is the most used material for photovoltaic applications. However, over the last decade, perovskite solar cells made from metal halide perovskite materials are cheaper and potentially more efficient than other thin-film solar cells [1]. Perovskite is one of the common crystal structures that can be found on Earth[2]. Due to its optimal structural and electronic properties, perovskites have received much attention in a variety of thematic areas and applications such as ferroelectricity, piezoelectricity, high-Tc superconductivity, ferromagnetism, giant magnetoresistance, photocatalysis, and photovoltaics [3]. The Pb-based hybrid perovskites ($APbI_3$) have been in focus in solar cell applications as they offer high power conversion efficiencies (PCE) comparable to the well-established Si-based solar cells where *A* could be an organic cation of $CH_3NH_3$ (Methylammonium) [4] or $(H_2N)_2CH^+$ (Formamidinium) [5]. Recent studies show that ($FAPbI_3$) formamidinium lead triiodide gives a high efficiency of 25.6% which is stable for 450 h [6]. $Pb^{2+}$ is responsible for unique optoelectronic properties of $APbI_3$ perovskites because of its 6 $s^2$, $p^0$ configuration, which results in lone 6 $s^2$ pairs and inactive $6p^0$ states [7] and also the high symmetry nature of lead halide perovskite. Nevertheless, the toxicity of lead and the long-term device stability issues are the major barriers to limiting its commercialization. Lead toxicity can be eliminated by replacing Pb with the other group cations. Apart from $Pb^{2+}$, $Tl^{3+,}$ and $Bi^{3+}$ also have the electronic configuration of 6 $s^2$ $6p^0$.

During the annealing process of $MAPbI_3$ ($M = CH_3$; $A = NH_3$), degradation is noted to occur at 85 °C in an inert atmosphere [9]. Experimentally, it is shown that mixing $MAPbI_3$ with a small quantity of inorganic cations such as $Cs^+$ with methylammonium ($CH_3$-$NH_3^+$)/formamidinium ($CH_3(NH_2)_2^+$) results in a photostable material [10]. Cs metal halides are thus of interest and these were first synthesized already in 1893, and $CsPbI_3$ and $CsPbBr_3$ are shown to have thermal stability up to the melting point of 460 °C [11]. This makes Cs based metal halides interesting, and Pb(II) ion could also be replaced with the combination of monovalent cation $Ag^+$ and trivalent cation $Bi^{3+}$. Most of the theoretical and experimental studies have been carried out with the inorganic

* Corresponding author.
*E-mail addresses:* ponniahv@kjemi.uio.no, vajeeston.ponniah@smn.uio.no (P. Vajeeston).

https://doi.org/10.1016/j.matpr.2022.06.063

Selection and peer-review under responsibility of the scientific committee of the Functional Materials for Energy, Environment and Biomedical Applications.

double perovskite of $Cs_2AgBiCl_6$ and $Cs_2AgBiBr_6$ [12]. All these studies are setup for optoelectronic applications which crystallize in cubic structure space group of Fm-3 m with an indirect bandgap. $Cs_2AgBiBr_6$ is shown to have good thermal and ambient stability without encapsulation[13]. A recent study reported that $Cs_2AgBiBr_6$ had high-hole mobility of 0.29 $cm^2s^{-1}V^{-1}$ in Field-Effect Transistor Applications [14]. However, there is limited discussion on the crystallography of $Cs_2AgBiBr_6$ and its impact on optoelectronic applications. In addition, the pressure[15] and the temperature[16] could influence the material to change its crystal structure and the electronic configuration. For example, at 122 K there is a phase transition between the room temperature cubic structure (Fm-3 m) and the low-temperature tetragonal phase(I4/m). This phase transition could affect the optical and electronic properties in terms of bandgap energies and the charge carrier lifetime[16]. At 4.5 GPa, cubic $Cs_2AgBiBr_6$ transfers to the tetragonal phase(I4/m) and they showed that beyond the 6.5Gpa the bandgap of the tetragonal phase narrows from 2.3 eV to 1.7 eV[15]. This leaves an interesting question regarding what structural changes we will see and how the optoelectronic properties would change in these phases.

## 2. Computational modelling

In this study, we focus on Cs2AgBiBr6, and the total energies of $Cs_2AgBiBr_6$ have been computed using the Vienna ab initio simulation package (VASP)[17]. The core states are described with potential generated through the projected augmented plane wave (PAW) method [18]. The exchange and correlation functions are treated within the GGA approach, using the approximation proposed by Perdew, Burke, and Ernzerhof (PBE)[19]. We optimized the atomic positions as well as the cell size and volume, minimizing both the stress tensor and the Hellman–Feynman forces with an overall force tolerance of $10^{-3}$ eV $Å^{-1}$. The HSE06 functional was used for computing the electronic structure. Our parameterization included a screened parameter of 0.2 $Å^{-1}$ and 30% mixing of the screened Hartree-Fock (HF) exchange with the PBE functional [20]. Fully converged results were obtained with a kinetic cut-off energy of 600 eV, and a 6 × 6 × 6 Γ-centered Monkhorst-Pack grids for integration over the Brillouin zone. This setting was used in both PBE and HSE06 calculations. The vibrational properties were computed with the frozen phonon approach, using suitably large supercell of the optimized structures. The Phonopy software was used to calculate the phonon dispersion curve and the associated density of states [21]. An atomic displacement of 0.0075 Å was used, and displacements in opposite directions were considered to improve the overall accuracy of the calculation of the force constants.

### 2.1. Structural stability

To understand the relative stability between cubic and tetragonal phases, we perform the geometry optimization by using the Murnaghan equation of fitting, in which the total energy of the unit cell is minimized concerning the cell volume within the DFT framework [22].

$$E = E_0 + \frac{B_0}{B_0'}(V - V_0) - \frac{B_0 V_0}{B_0'(1 - B_0')}\left[\left(\frac{V}{V_0}\right)^{1-B_0'} - 1\right] \quad (1)$$

Where V is the primitive-cell volume, B is the bulk modulus, which provides the behavior of the crystal volume under hydrostatic pressure[23], and B' is its first pressure derivative. The zero indexes are the values at zero pressure[24].

The structural stability of the cubic and tetragonal phases has been studied with the GGA-PBE method.

The calculated energy volume curve clearly indicates that the tetragonal phase has a lower ground state energy than the cubic phase, see Fig. 1. This means the tetragonal phase of $Cs_2AgBiBr_6$ is more structurally stable than the cubic phase. The computed lattice parameters are given in below Table1.

#### 2.1.1. Dynamical stability

To understand the dynamical stability of the studied polymorphs of $Cs_2AgBiBr_6$, we carried out phonon calculations and these are the first such results reported. In addition to the total phonon density of states (PDOS), we also calculated the phonon dispersion curves, at the equilibrium volume. Along the high symmetry direction of the Brillouin zone for cubic and tetragonal variations are presented in Fig. 2 with their corresponding PDOS. From our study, we found that for the tetragonal structure all phonon modes are positive and this structure is dynamically stable. On the other hand, the cubic structure has several negative modes especially G-X, K-G-L, and U-X, and the cubic phase is dynamically unstable.

#### 2.1.2. Mechanical stability

Material's mechanical behavior could be explained by the elastic modulus. The relationship between the stress and strain can be described by Constitutive law within the elastic region and it can be simplified in Voigt notation [29].

$$\sigma_i = \sum_{j=1}^{6} c_{ij}\varepsilon_{ij} \quad (2)$$

The elastic constants describe the response to an applied force, as either applied strain or the required stress to maintain a certain deformation. Both stress and strain have three tensile and three shear components. Due to this, the elastic constants of a crystal can be described using a 6 × 6 symmetric matrix, having 27 components where 21 of which are independent [30]. Naturally, we can reduce the number of components by utilizing any existing symmetry in the material. A cubic crystal has only three independent

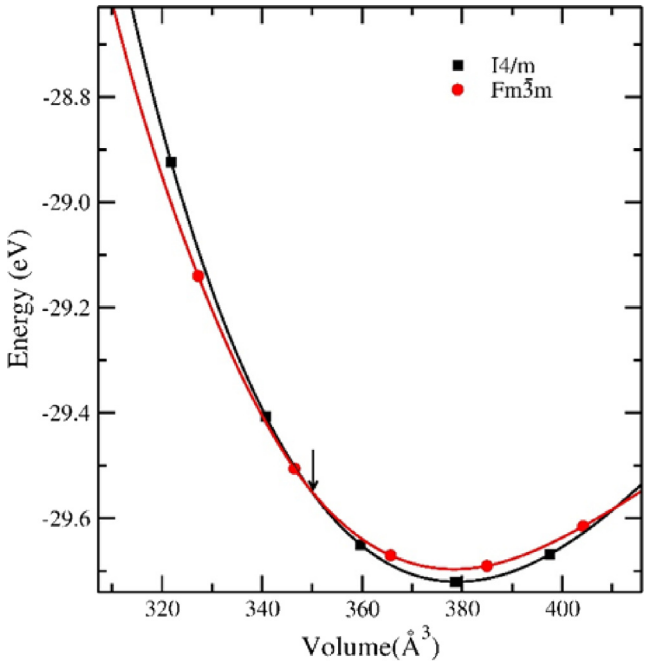


**Fig. 1.** The total energy as a function of the volume of $Cs_2AgBiBr_6$ halide double perovskite in cubic and tetragonal phases.

**Table 1**
Obtained equilibrium lattice parameters (in Å), using GGA.

| | $Cs_2AgBiBr_6$(Fm-3 m) | $Cs_2AgBiBr_6$(I4/m) |
|---|---|---|
| a | 11.4836,11.462[25], 11.25[26],11.53 [27],11.271[28] | 8.0428,7.844[25],7.879 [16] |
| c | | 11.6667,11.425 [25],11.323[16] |
| Volume/ Å$^3$ | 378 | 385 |

elastic constants (C11, C12, and C44), each of which is representative of three deformations ($C_{12} = C_{13}$, $C_{11} = C_{33} = C_{31}$, $C_{44} = C_{66}$) [31]. The mechanical stability criteria is given as [25].

$$C_{44} > 0;\ C_{11} > C_{12};\ C_{11} + 2\ C_{12} > 0 \quad (3)$$

Cubic structure of $Cs_2AgBiBr_6$ fulfills mechanical stability criteria.

Tetragonal phase ($C_{11}$, $C_{33}$, $C_{44}$, $C_{66}$, $C_{12,}$ and $C_{13}$)and its mechanical stability criteria [25] are discussed below and tetragonal structure of $Cs_2AgBiBr_6$ too satisfies the criteria.

$$C_{11} > 0,\ C_{33} > 0,\ C_{44} > 0,\ C_{66} > 0, C_{11} - C_{12} > 0,\ C_{11} + C_{33} - 2C_{13} > 0, 2(C_{11} + C_{12}) + C_{33} + 4C_{13} > 0 \quad (4)$$

Similar to the elastic constant tensor, the bulk (Bv, $B_R$) and the shear moduli (Gv, $G_R$) provide information regarding the material hardness under deformation. These parameters are computed for the considered phases of $Cs_2AgBiBr_6$ and listed in Table2. These properties can be directly computed from the elastic constants tensors. Using Pugh's criterion which is based on the value B/G ratio, we could determine whether the material is ductile or brittle. When B/G > 1.75, it shows the character of ductility and when it is less than 1.75, the material shows brittle character. Our calculations show that $Cs_2AgBiBr_6$ is ductile in both phases[25].

### 2.2. Electronic properties

The bandstructure of $Cs_2AgBiBr_6$ was calculated, to investigate whether it is an insulator, a conductor, or a semiconductor. Electronic calculations were done using GGA and HSE06 methods. The band structures E(k) were computed on a discrete k mesh along with the high-symmetry directions in the Brillouin zone (BZ).

**Table 2**
The calculated single-crystal elastic constants Cij (in GPa), bulk modulus B (in GPa), shear modulus G (in GPa), Poisson's ratio (v), Young's modulus E (in GPa), Pugh's indicator B/G and Debye temperature ($T_D$, in K) for $Cs_2AgBiBr_6$ phases. Subscript V indicates the Voigt bound, R indicates the Reuss bound, and H indicates the Hill average.

| Phase | $Cs_2AgBiBr_6$ | |
|---|---|---|
| | Cubic | Tetragonal |
| $C_{ij}$ | $C_{11}$ = 25.409, 59.02[32],44.05[33],47.94[25], 38.74[34]<br>$C_{12}$ = 14.483, 13.37[32], 16.36[33], 10.75 [25],7.58[34]<br>$C_{44}$ = 6.301,8.15[32],6.56[33],5.13[25],7.46 [34] | $C_{11}$ = 23.826, 44.76 [25]<br>$C_{12}$ = 13.449, 32.02 [25]<br>$C_{13}$ = 13.802, 16.85 [25]<br>$C_{33}$ = 24.311, 62.75 [25]<br>$C_{44}$ = 4.237, 8.81 [25]<br>$C_{66}$ = 3.139, 11.62 [25] |
| $B_v$ | 18.13 | 17.12 |
| $B_R$ | 18.125 | 17.039 |
| $B_H$ | 18.125, 25.59[33] | 17.079 |
| $G_v$ | 5.97 | 4.38 |
| $G_R$ | 5.937 | 3.680 |
| $G_H$ | 5.951,8.89[33] | 4.032 |
| $E_V$ | 16.13 | 12.12 |
| $E_R$ | 16.057 | 10.298 |
| $E_H$ | 16.092 | 11.213 |
| $v_v$ | 0.35 | 0.38 |
| $v_R$ | 0.352 | 0.399 |
| $v_H$ | 0.352 | 0.391 |
| (B/G) | 3.04 | 4.24 |
| $T_D$ | 112.7,136[33],137.08[25] | 93.2,138.456[25], 114[35] |

In Fig. 3, we can clearly see that both $Cs_2AgBiBr_6$ phases are semiconductors with an indirect bandgap. The lowest of the conduction band (CBM) lies at the L-point whereas the valence band maxima (VBM) lies at X point in cubic phase materials. For the tetragonal phase, CBM lies at X and VBM lies at L high symmetric points in the first BZ. As expected the band gap values obtained with GGA are underestimations, thus we perform more accurate calculations with HSE06 [36]. When the symmetry of the material decreases from cubic to tetragonal phase, the bandgap value increases, which proven by our computed electronic bandgaps in Table 3 of both the cubic and tetragonal phases of $Cs_2AgBiBr_6$. This

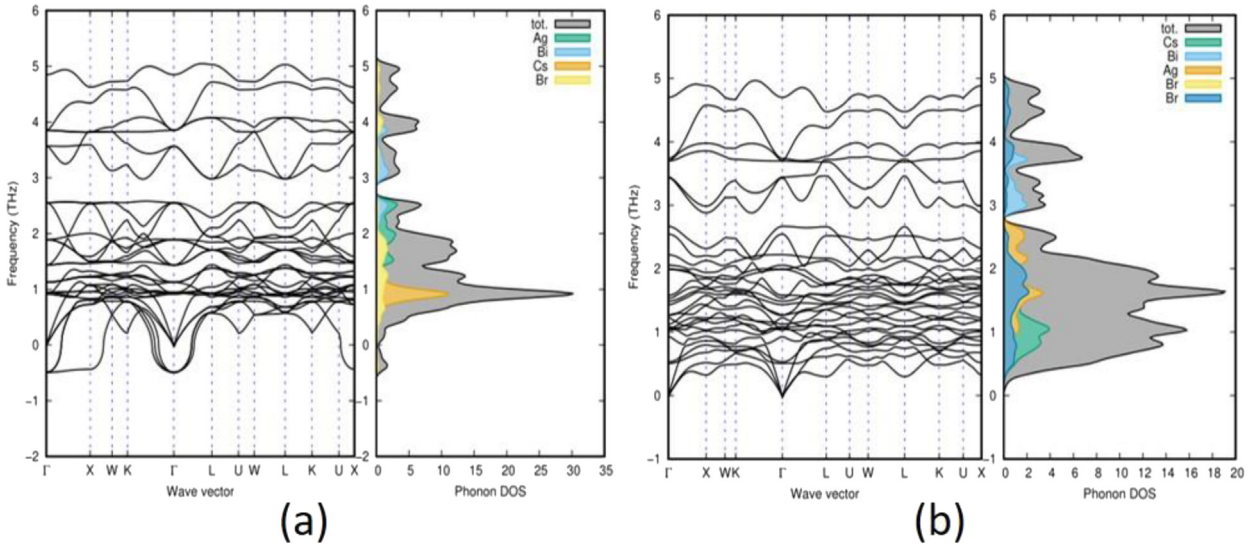


**Fig. 2.** Phonon dispersion curves of $Cs_2AgBiBr_6$ halide double perovskite for **a** cubic and **b** tetragonal phases.

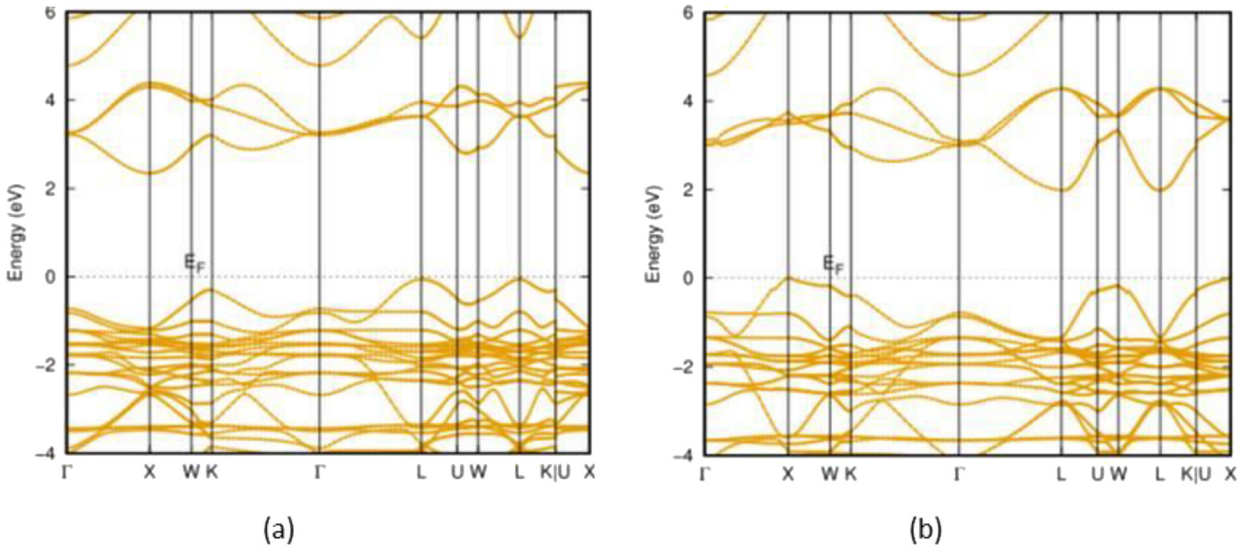


**Fig. 3.** Band diagrams of $Cs_2AgBiBr_6$ halide double perovskite for **a** cubic and **b** tetragonal phases.

**Table 3**
Calculated bandgaps (eV) of $Cs_2AgBiBr_6$ halide double perovskite (cubic and tetragonal phases) using GGA and HSE06.

| | $Cs_2AgBiBr_6$(Fm-3 m) | $Cs_2AgBiBr_6$(I4/m) |
|---|---|---|
| **GGA** | **1.35,** 1.42[22], 1.26[25] | **1.49**, 2.06[25] |
| **HSE06** | **1.97,** 2.06[38], 1.79[39] 2.59, 1.34, 2.4[40] 1.98[41] | **2.4,** 2.3[15] |

indicates that structural distortion and symmetry deterioration lead to bandwidth narrowing and energetic stability[37] (See Table 4.).

The electrons' motion can be described with the definite position and momentum under the assumption of all moving charge carriers that are close to the band edge in terms of a semi-classical approach. We could explain the mobility of moving charge carriers using effective mass (m*) as it is a quantity that is used to simplify band structures by modeling the behavior of a free particle with that mass. This formula was derived by using approximations in Taylor's series expansion at the band edge in the region of parabolic fitting[42].

$$m^* = \hbar^2 \left( \frac{d^2E}{dK^2} \right)^{-1} \tag{5}$$

m* is the effective mass of the charge carrier, k is the wave vector, ħ is the reduced Planck constant and E is the energy of an electron at wave vector k in that band. The parabolic nature (second derivate) of the bandstructure plot, reveals which one of the structures that will have the highest electron mobility as the second derivative and the effective mass are inversely proportional. In Fig. 3, the bandstructures of HSE06 show a high dispersive (large second derivative) of the CBM compared to the VBM. This indicates a lower effective mass of electrons compared to the effective mass of the holes. Using the transfer rate of charge carriers (v), we can discover the nature of the mobility or conductivity based on the following equation.

$$v = \frac{\hbar k}{m^*} \tag{6}$$

As the equation illustrates, electron mass increases when the mobility is reduced, and vice versa. Our calculations show that both $Cs_2AgBiBr_6$ structures have higher electron mobility ($m_e$) compared to hole mobility ($m_h$). Effective mass calculations for both cubic and tetragonal structures are presented in different directions in the BZ.

**Table 4**
Effective masses ($m_e$, $m_h$) calculated for cubic and tetragonal $Cs_2AgBiBr_6$ double perovskite using GGA approximation.

| Direction | $Cs_2AgBiBr_6$(Fm-3 m) | | $Cs_2AgBiBr_6$(I4/m) | |
|---|---|---|---|---|
| | $m_e^*/m_o$ | $m_h^*/m_o$ | $m_e^*/m_o$ | $m_h^*/m_o$ |
| (G → K) | 0.376 | 0.447 | 1.020 | 0.293 |
| (G → L) | 0.310 | 0.366 | 1.027 | 0.364 |
| (G → X) | 0.328 | 0.678 | 1.566 | 0.421 |

### 2.3. Chemical bonding

To gain a better understanding of bonding interactions, the calculated valence-charge-density distribution was used. Both cubic and tetragonal polymorphs are having almost a similar feature as shown in Fig. 4. According to the charge-density distribution at the Cs, Ag, Bi, and Br sites, it is evident that the highest charge density resides in the immediate vicinity of the nuclei. As also evidenced from the almost spherical charge distribution, the bonding between Cs and Br is virtually pure ionic and between Cs-Br is predominantly ionic. The type of charge distribution seen in Fig. 4 (b–d) appears to be typical for ionic compounds. On the other hand, the charge distribution at the Ag, Br, and Bi sites are of non-spherical nature and the considerable charges are shared between the Ag-Br, and Bi-Br atoms (see Fig. 4 a and c), which implies that there must be a significant amount of covalent character in the Bi-Br, Ag-Br bonds. Fig. 4 (e–h) depicts the charge transfer (i.e., the electron distribution in the compound minus the electron density of the corresponding overlapping free atoms) in $Cs_2AgBiBr_6$. This illustration further reconfirms that the charge has been depleted from the Cs and Ag sites and are transferred to the Br sites. The overall message is that $Cs_2AgBiBr_6$ is to be regarded as a mixed bonding substance.

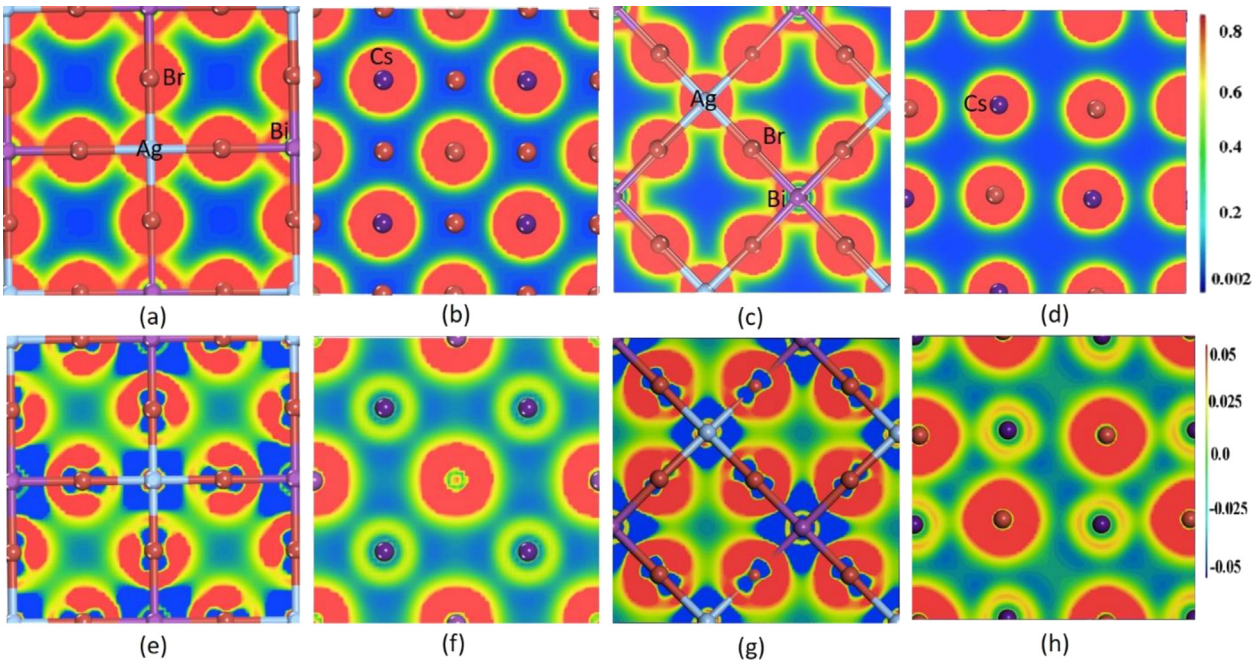


**Fig. 4.** Calculated charge density (a–d), and charge transfer (e–h), plots along (1 0 0) for $Cs_2AgBiBr_6$ in the cubic (charge density a, b; charge transfer e, f) and tetragonal (charge density c, d; charge transfer g, h) structure.

## 3. Conclusion

Structural stability, electronic structure, and chemical bonding of the cubic and tetragonal phase of $Cs_2AgBiBr_6$ were investigated using the PAW potential method by adopting the first principle calculations.

The main results obtained are as follows:

- Tetragonal phase of $Cs_2AgBiBr_6$ is found to be more stable than its cubic blende phase.
- The phonon calculations reveal that the tetragonal structure of $Cs_2AgBiBr_6$ is found to be dynamically stable while the cubic structure shows the negative frequency making it dynamically unstable.
- The single crystal elastic tensor calculations show that both phases are mechanically stable and both are ductile.
- Our band structure calculations show that the $Cs_2AgBiBr_6$ polymorphs are semiconductors with indirect bandgaps.
- Our calculations show cubic and tetragonal phases of $Cs_2AgBiBr_6$ that have the potential to be used in flexible optoelectronic applications

## CRediT authorship contribution statement

**W.A. Chapa Pamodani Wanniarachchi:** Conceptualization, Software, Investigation, Writing – original draft. **Håkon Eidsvåg:** Writing – review & editing. **Thevakaran Arunasalam:** Conceptualization, Supervision. **Punniamoorthy Ravirajan:** Conceptualization, Writing – review & editing, Supervision, Project administration, Funding acquisition. **Dhayalan Velauthapillai:** Funding acquisition, Supervision, Conceptualization, Writing – review & editing, Project administration. **Ponniah Vajeeston:** Supervision, Conceptualization, Methodology, Software, Investigation, Writing – review & editing.

## Declaration of Competing Interest

The authors declare that they have no known competing financial interests or personal relationships that could have appeared to influence the work reported in this paper.

## Acknowledgments

This research was funded by the the Capacity Building and Establishment of Research Consortium (CBERC), grant number LKA-3182-HRNCET, and Higher Education and Research collaboration onNanomaterials for Clean Energy Technologies (HRNCET) project, Grant Number NORPART/2016/10237.

The authors gratefully acknowledge the Research Council of Norway for providing the computer time (project number NN2867k) at the Norwegian supercomputer facility.

## References:

[1] T. Leijtens, G.E. Eperon, N.K. Noel, S.N. Habisreutinger, A. Petrozza, H.J. Snaith, Stability of metal halide perovskite solar cells, Adv. Energy Mater. 5 (20) (2015) Oct, https://doi.org/10.1002/AENM.201500963.
[2] R. M. Hazen, S. S. American, and N. June, "Perovskites gives rise to materials that have a wide array of electrical properties," *Sci. Am.*, vol. 258, no. 6, pp. 74–81, 1988, [Online]. Available: http://www.jstor.org/stable/24989124
[3] G. Volonakis, M.R. Filip, A.A. Haghighirad, N. Sakai, B. Wenger, H.J. Snaith, F. Giustino, Lead-free halide double perovskites via heterovalent substitution of noble metals, J. Phys. Chem. Lett. 7 (7) (2016) 1254–1259, https://doi.org/10.1021/acs.jpclett.6b00376.
[4] A. Kojima, K. Teshima, Y. Shirai, T. Miyasaka, Organometal halide perovskites as visible-light sensitizers for photovoltaic cells, J. Am. Chem. Soc. 131 (17) (2009) 6050–6051, https://doi.org/10.1021/ja809598r.
[5] A.M. Peir?, P. Ravirajan, K. Govender, D.S. Boyle, P. O'Brien, D.D.C. Bradley, J. Nelson, J.R. Durrant, Hybrid polymer/metal oxide solar cells based on ZnO columnar structures, J. Mater. Chem. 16 (21) (2006) 2088.
[6] J. Werner, "Perovskite/Silicon Tandem Solar Cells: Toward Affordable Ultra-High Efficiency Photovoltaics ?," vol. 8659, pp. 1–161, 2018
[7] E. S.-P. review and undefined 1926, "An undulatory theory of the mechanics of atoms and molecules," *APS*, Accessed: Apr. 17, 2020. [Online]. Available: https://journals.aps.org/pr/abstract/10.1103/PhysRev.28.1049.
[9] B. Conings *et al.*, "Intrinsic Thermal Instability of Methylammonium Lead Trihalide Perovskite," 2015, doi: 10.1002/aenm.201500477

[10] D.P. McMeekin, G. Sadoughi, W. Rehman, G.E. Eperon, M. Saliba, M.T. Hörantner, A. Haghighirad, N. Sakai, L. Korte, B. Rech, M.B. Johnston, L.M. Herz, H.J. Snaith, A mixed-cation lead mixed-halide perovskite absorber for tandem solar cells, Science 351 (6269) (2016) 151–155.
[11] R.J. Sutton, G.E. Eperon, L. Miranda, E.S. Parrott, B.A. Kamino, J.B. Patel, M.T. Hörantner, M.B. Johnston, A.A. Haghighirad, D.T. Moore, H.J. Snaith, Bandgap-tunable cesium lead halide perovskites with high thermal stability for efficient solar cells, Adv. Energy Mater. 6 (8) (2016) 1502458.
[12] M. R. Filip, S. Hillman, A. Haghighirad, H. J. Snaith, and F. Giustino, "Band Gaps of the Lead-Free Halide Double Perovskites Cs 2 BiAgCl 6 and Cs 2 BiAgBr 6," 2016, doi: 10.1021/acs.jpclett.6b01041.
[13] C. Wu *et al.*, "CommuniCation The Dawn of Lead-Free Perovskite Solar Cell: Highly Stable Double Perovskite Cs 2 AgBiBr 6 Film," 2017, doi: 10.1002/advs.201700759
[14] G. Abiram, F. Heidari Gourji, S. Pitchaiya, P. Ravirajan, T. Murugathas, and D. Velauthapillai, "Air processed Cs 2 AgBiBr 6 lead-free double perovskite high-mobility thin-film field-effect transistors," 123AD, doi: 10.1038/s41598-022-06319-z
[15] Q. Li, Y. Wang, W. Pan, W. Yang, B.o. Zou, J. Tang, Z. Quan, High-pressure band-gap engineering in lead-free Cs 2 AgBiBr 6 double perovskite, Angew. Chem. 129 (50) (2017) 16185–16189, https://doi.org/10.1002/ange.201708684.
[16] L. Schade *et al.*, "Structural and Optical Properties of Cs 2 AgBiBr 6 Double Perovskite," vol. 2, p. 14, 2022, doi: 10.1021/acsenergylett.8b02090
[17] G. Kresse, D. Joubert, From ultrasoft pseudopotentials to the projector augmented-wave method, Phys. Rev. B - Condens. Matter Mater. Phys. 59 (3) (1999) 1758–1775, https://doi.org/10.1103/PhysRevB.59.1758.
[18] Q. Xu *et al.*, "SPARC: Simulation Package for Ab-initio Real-space Calculations," *SoftwareX*, vol. 15, p. 100709, 2021, doi: 10.1016/j.softx.2021.100709.
[19] J.P. Perdew, K. Burke, M. Ernzerhof, Generalized gradient approximation made simple, Phys. Rev. Lett. 77 (18) (1996) 3865–3868, https://doi.org/10.1103/PhysRevLett.77.3865.
[20] J. Heyd, G.E. Scuseria, Efficient hybrid density functional calculations in solids: assessment of the Heyd-Scuseria-Ernzerhof screened Coulomb hybrid functional ARTICLES YOU MAY BE INTERESTED IN, J. Chem. Phys. 121 (3) (2004) 1187–1192, https://doi.org/10.1063/1.1760074.
[21] A. Togo, I. Tanaka, First principles phonon calculations in materials science, Scripta Mater. 108 (2015) 1–5, https://doi.org/10.1016/j.scriptamat.2015.07.021.
[22] N. Rajeev Kumar, R. Radhakrishnan, Electronic, optical and mechanical properties of lead-free halide double perovskites using first-principles density functional theory, Mater. Lett. 227 (2018) 289–291, https://doi.org/10.1016/j.matlet.2018.05.082.
[23] S. Wu, S.S. Naghavi, G.H. Fecher, C. Felser, A critical study of the elastic properties and stability of heusler compounds: phase change and tetragonal X<sub>2</sub>YZ compounds, J. Mod. Phys. 09 (04) (2018) 775–805, https://doi.org/10.4236/jmp.2018.94050.
[24] C. M. You, "Periodic Hartree-Fock linear combination of crystalline orbitals calculation of the structure , equation of state and elastic properties of titanium diboride Periodic Hartree – Fock linear combination of crystalline orbitals calculation of the structure ," 2000.
[25] T. Bellakhdar, Z. Nabi, B. Bouabdallah, B. Benichou, H. Saci, Ab initio study of structural, electronic, mechanical and optical properties of the tetragonal Cs2AgBiBr6 halide double perovskite, Appl. Phys. A 128 (2) (2022), https://doi.org/10.1007/s00339-022-05276-8.
[26] A.H. Slavney, T. Hu, A.M. Lindenberg, H.I. Karunadasa, A bismuth-halide double perovskite with long carrier recombination lifetime for photovoltaic applications, J. Am. Chem. Soc. 138 (7) (2016) 2138–2141, https://doi.org/10.1021/jacs.5b13294.
[27] N.R. Kumar, R. Radhakrishnan, Electronic, optical and mechanical properties of lead-free halide double perovskites using first-principles density functional theory, Mater. Lett. 227 (2018) 289–291, https://doi.org/10.1016/j.matlet.2018.05.082.
[28] E.T. McClure, M.R. Ball, W. Windl, P.M. Woodward, Cs2AgBiX6 (X = Br, Cl): new visible light absorbing, lead-free halide perovskite semiconductors, Chem. Mater. 28 (5) (Mar. 2016) 1348–1354, https://doi.org/10.1021/acs.chemmater.5b04231.
[29] N. Xu, "VASPKIT : A User-friendly Interface Facilitating High-throughput Computing and Analysis Using VASP Code," no. August 2019, 2021.
[30] P. Vajeeston, H. Fjellvåg, First-principles study of structural stability, dynamical and mechanical properties of Li 2 FeSiO 4 polymorphs, RSC Adv. 7 (27) (2017) 16843–16853.
[31] M. Rasukkannu, D. Velauthapillai, and P. Vajeeston, "Hybrid Density Functional Study of Au 2 Cs 2 I 6 ," no. December, 2018, doi: 10.3390/en11123457.
[32] L. Dong, S. Sun, Z. Deng, W. Li, F. Wei, Y. Qi, Y. Li, X. Li, P. Lu, U. Ramamurty, Elastic properties and thermal expansion of lead-free halide double perovskite Cs2AgBiBr 6, Comput. Mater. Sci. 141 (2018) 49–58, https://doi.org/10.1016/J.COMMATSCI.2017.09.014.
[33] N. Guechi, A. Bouhemadou, S. Bin-omran, A. Bourzami, L. Louail, and F. Abbas Setif, "Elastic, Optoelectronic and Thermoelectric Properties of the Lead-Free Halide Semiconductors Cs2AgBiX 6 (X = Cl, Br): Ab Initio Investigation," *J. Electron. Mater.*, vol. 47, 1900, doi: 10.1007/s11664-017-5962-2.
[34] M.N. Islam, J. Podder, T. Saha, P. Rani, Semiconductor to metallic transition under induced pressure in Cs 2 AgBiBr 6 double halide perovskite: a theoretical DFT study for photovoltaic and optoelectronic applications, RSC Adv. 11 (39) (2021) 24001–24012, https://doi.org/10.1039/d1ra03161a.
[35] L. S. J. Zelewski, y, z J. M. Urban, y A. Surrente, y D. K. Maude, y A. Kuc, x P. Schade, x R. D. Johnson, x M. Dollmann, x P. K. Nayak, x H. J. Snaith, y and M. Radaelli, x R. Kudrawiec, z R. J. Nicholas, x P. Plochocka, and Baranowski, "Revealing the nature of photoluminescence emission in the metal-halide double perovskite Cs2AgBiBr6," *Mater. Chem. C*, vol. 7, pp. 8350–8356, 2019.
[36] P. Borlido, T. Aull, A.W. Huran, F. Tran, M.A.L. Marques, S. Botti, Large-Scale benchmark of exchange–correlation functionals for the determination of electronic band gaps of solids, J. Chem. Theory Comput. 15 (9) (2019) 5069–5079, https://doi.org/10.1021/acs.jctc.9b00322.
[37] T. Umebayashi, K. Asai, T. Kondo, A. Nakao, Electronic structures of lead iodide based low-dimensional crystals, Phys. Rev. B - Condens. Matter Mater. Phys. 67 (15) (2003), https://doi.org/10.1103/PhysRevB.67.155405.
[38] E.T. McClure, M.R. Ball, W. Windl, P.M. Woodward, Cs2AgBiX6 (X = Br, Cl): new visible light absorbing, lead-free halide perovskite semiconductors, Chem. Mater. 28 (5) (2016) 1348–1354, https://doi.org/10.1021/acs.chemmater.5b04231.
[39] C.N. Savory, A. Walsh, D.O. Scanlon, Can Pb-free halide double perovskites support high-efficiency solar cells?, ACS Energy Lett 1 (5) (2016) 949–955, https://doi.org/10.1021/acsenergylett.6b00471.
[40] M.A. Ghebouli, T. Chihi, B. Ghebouli, M. Fatmi, Study of the structural, elastic, electronic and optical properties of lead free halide double perovskites Cs2AgBiX6(X = Br, Cl), Chinese J. Phys. 56 (1) (2018) 323–330, https://doi.org/10.1016/j.cjph.2018.01.004.
[41] G. Liu *et al.*, "Extending Absorption of Cs 2 AgBiBr 6 to Near-Infrared Region (≈1350 nm) with Intermediate Band," 2021, doi: 10.1002/adfm.202109891
[42] D. Akinwande, Y. Nishi, H.-S.-P. Wong, An analytical derivation of the density of states, effective mass, and carrier density for achiral carbon nanotubes, IEEE Trans. Electron Devices 55 (1) (2008) 289, https://doi.org/10.1109/TED.2007.911078.

## *Further reading*

[8] R. Mohan, "Green bismuth," 2010. doi: 10.1038/nchem.609.